

Article

# Facile Preparation of $\text{BaCl}_x\text{F}_y$ for the Catalytic Dehydrochlorination of 1-Chloro-1,1-Difluoroethane to Vinylidene Fluoride

Wei Yu , Wenfeng Han \* , Yongnan Liu, Jiaqin Lu, Hong Yang, Bing Liu, Haodong Tang, Aimin Chen and Ying Li

Industrial Institute of Catalysis, Zhejiang University of Technology, Hangzhou 310032, China; WillYmt1989@outlook.com (W.Y.); Yongnan\_Liu@126.com (Y.L.); jiaqin\_lu@126.com (J.L.); hongyang\_zjut@163.com (H.Y.); bing\_liu\_zjut@126.com (B.L.); tanghd@zjut.edu.cn (H.T.); amchen@zjut.edu.cn (A.C.); liying@zjut.edu.cn (Y.L.)

\* Correspondence: hanwf@zjut.edu.cn

Received: 28 February 2020; Accepted: 19 March 2020; Published: 1 April 2020



**Abstract:**  $\text{BaCl}_x\text{F}_y$  as well as  $\text{BaF}_2$  and  $\text{BaClF}$  catalysts were prepared by solid-state reaction at room temperature with  $\text{Ba}(\text{OH})_2$  as the precursor and  $\text{NH}_4\text{F}/\text{NH}_4\text{Cl}$  as the F and Cl sources. The catalysts were applied for the dehydrochlorination of 1-chloro-1,1-difluoroethane to vinylidene fluoride at 350 °C. The industrial manufacture of vinylidene fluoride (VDF) is carried out at 600–700 °C, whereas the  $\text{BaCl}_x\text{F}_y$  catalysts provided a promising pathway to produce VDF at much lower temperatures. Unfortunately, the selectivity of VDF over  $\text{BaF}_2$  decreased from 94% to 84% along with the deactivation of the  $\text{BaF}_2$  catalyst monotonically. In the presence of small amounts of Cl in  $\text{BaF}_2$ , stabilized selectivity was achieved. Over  $\text{BaCl}_{0.05}\text{F}_{0.95}$ ,  $\text{BaCl}_{0.1}\text{F}_{0.9}$  and  $\text{BaCl}_{0.25}\text{F}_{0.75}$ , no decrease in VDF selectivity was observed. Clearly, the presence of small amounts Cl during solid-state preparation inhibited the growth of  $\text{BaF}_2$  crystalline significantly. Far smaller particles were achieved. The particle size, or more precisely, the crystal size of the barium catalyst played a major role in the catalytic performance. In addition to the crystal growth, the presence of small amounts of Cl during catalyst preparation changed the chemical state of Ba, and therefore the adsorption and activation of the C–Cl bond for HCFC-142b were altered.

**Keywords:** barium chlorofluoride; catalytic pyrolysis; barium fluoride; dehydrochlorination; 1-chloro-1,1-difluoroethane; vinylidene fluoride

## 1. Introduction

1,1-difluoroethylene (VDF) is one of the major fluoromonomers, which are the feedstock for the production of various resins, rubbers membrane and paints [1]. The polymers derived from VDF (PVDF) or co-polymers with unique chemical resistance, stability at elevated temperatures, oxidation resistance, weatherability, piezoelectricity, dielectric and thermoelectricity, find wide applications in areas including petrochemical, electronic and electrical, and fluorocarbon coating [2]. VDF is the second largest product among fluorocarbons with an annual production capacity of above 53,000 tons. The demand for VDF is increasing rapidly. At present, in industry, VDF is usually produced via the dehydrochlorination of 1,1-difluoro-1-chloroethane (HCFC-142b) at reaction temperatures above 650 °C [3,4]. Dehydrochlorination is an efficient route for the preparation of 1, 1-dichloroethylene (VDC), vinyl chloride monomer (VCM), 2,3,3,3-tetrafluoropropene (HFO-1234yf), and ethylene oxychlorination [5–8]. As the dehydrochlorination of HCFC-142b is a highly endothermic reaction, very long reaction tubes are adopted to supply the reaction heat. Unfortunately, this also leads to the

generation of carbon deposition during the reaction process at elevated temperatures. Consequently, the reactor needs to be cut off to remove the coke after a period of reaction, which significantly reduces the efficiency of continuous production.

We have reported that the dehydrochlorination of HCFC-142b is promoted by catalysts such as N-doped activated carbon [9], N-containing mesoporous carbon [10], and metal fluorides [3,4]. The presence of catalysts reduces the reaction temperature from 650 °C to lower than 350 °C, facilitating saving energy consumption and avoiding the formation of coke during reaction. Although N-doped activated carbon and mesoporous carbon materials exhibit a moderate conversion of HCFC-142b and high selectivity to VDF, they are difficult to recover following deactivation by coking. SrF<sub>2</sub> shows a high activity for the pyrolysis of HCFC-142b to VDF under moderate conditions. However, its selectivity and stability are rather low [4]. Although the preparation of SrF<sub>2</sub> microparticles with cubic structures improves the performance, the procedure is complicated and it is difficult to scale-up.

Due to the formation of highly corrosive byproducts, HCl and HF, during pyrolysis of HCFC-142b, there are very rare choices for the exploration of proper materials as the catalysts. Therefore, carbon materials and metal fluorides which are HF-corrosion-resistant are the potential catalysts. In addition to carbon materials, metal fluorides were also systematically investigated for the catalytic pyrolysis of HCFC-142b [11]. Among the various metal fluorides, barium fluoride shows relatively high activity in this reaction, with selectivity to VDF of 95% [11]. Other metal fluorides, such as MgF<sub>2</sub>, AlF<sub>3</sub> and fluorinated Cr<sub>2</sub>O<sub>3</sub> were found to be catalysts for dehydrofluorination reactions [12–14]. Similar to the chlorination of AlF<sub>3</sub> to aluminum chlorofluoride (ACF), BaF<sub>2</sub> also tends to be chlorinated to BaClF by Cl species under reaction conditions [15]. Consequently, a rapid decrease in the conversion of HCFC-142b and selectivity to VDF was observed. In a similar reaction system for dehydrofluorination, which was catalyzed by AlF<sub>3</sub>, strong Lewis acid promoted both dehydrofluorination and coke deposition. As a result, a fast deactivation was seen. It was reported that the pre-deposition of carbon prior to reaction leads to the partial coverage of strong Lewis acid sites and improves the stability of catalysts [16]. As reported previously, BaF<sub>2</sub> converts to BaClF via reaction with HCl at reaction temperatures, resulting in the deactivation of the catalyst [11,17]. Clearly, the inhibition of chlorination of the BaF<sub>2</sub> catalyst by Cl species is one of the key challenges for the catalytic pyrolysis of HCFC-142b.

In this study, barium fluoride was pre-chlorinated to barium chlorofluoride during the preparation of the catalyst. BaCl<sub>x</sub>F<sub>y</sub> catalysts were prepared by solid-state reaction at room temperature with various molar ratios of Cl and F. The catalysts were applied for the pyrolysis of 1-chloro-1,1-difluoroethane to vinylidene fluoride. The effect of Cl composition on the performance of the BaF<sub>2</sub> catalyst for catalytic pyrolysis was investigated.

## 2. Results

The catalytic performance of barium chlorofluoride for the pyrolysis of 1-chloro-1,1-difluoroethane (CH<sub>3</sub>CClF<sub>2</sub>, HCFC-142b) to vinylidene fluoride (VDF, CH<sub>2</sub>=CF<sub>2</sub>) as a function of time-on-stream is shown in Figure 1. The reactions were carried out at atmospheric pressure, a gas hourly space velocity (GHSV) of 1200 h<sup>-1</sup>, and a reaction temperature of 350 °C. As expected, BaCl<sub>2</sub> is rather inactive for the pyrolysis of HCFC-142b. However, consistent with our previous study, BaF<sub>2</sub> is efficient for the promotion of pyrolysis [11]. In addition to VDF, vinylidene chlorofluoride (CH<sub>2</sub>=CClF, VCF) via dehydrofluorination was detected as the major carbon-containing by-product. As indicated in Figure 1a, the conversion of HCFC-142b over BaClF is only around 10%, which is significantly lower than that of BaF<sub>2</sub> (40%–60%). Hence, it is reasonable for the gradual deactivation of BaF<sub>2</sub> catalysts following the chlorination to BaClF or BaCl<sub>2</sub>.

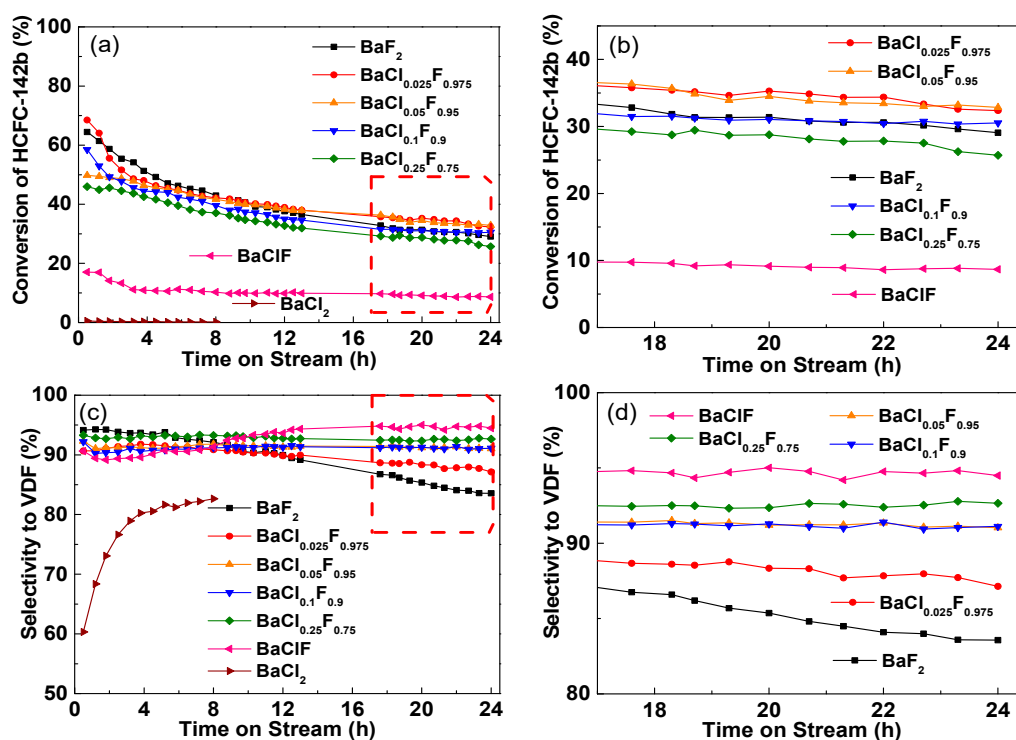


**Figure 1.** Catalytic performance of  $BaCl_xF_y$  catalysts for the pyrolysis of HCFC-142b as a function of time on stream at atmospheric pressure, a gas hourly space velocity (GHSV) of  $1200\text{ h}^{-1}$ , and a reaction temperature of  $350\text{ }^\circ\text{C}$ . (a) Conversion of HCFC-142b, (b) Highlighted conversion of HCFC-142b for the time on stream between 14 and 24 h, (c) Selectivity to vinylidene fluoride (VDF) and (d) Highlighted selectivity to VDF for the time on stream between 14 and 24 h.

Different from the catalysts of  $BaF_2$ ,  $BaCl_2$  and  $BaClF$ , doping of small amounts of Cl to  $BaF_2$  forming  $BaCl_xF_y$  changes the conversion of HCFC-142b slightly. Compared with  $BaF_2$ , with a doping amount of less than 10%, the conversion levels are improved, while, with increased amounts, a similar or even lower conversion results (Figure 1b).

Unexpectedly, the doping of small amounts of Cl to  $BaF_2$  significantly enhances the selectivity to VDF (Figure 1c). For the  $BaF_2$  catalyst, the selectivity of VDF decreases from 94% to 84% along with the deactivation of  $BaF_2$  catalyst monotonically (Figure 1c). In the presence of small amounts of Cl in  $BaF_2$ , stabilized selectivity is achieved. Over  $BaCl_{0.05}F_{0.95}$ ,  $BaCl_{0.1}F_{0.9}$  and  $BaCl_{0.25}F_{0.75}$ , no decrease in VDF selectivity is observed (Figure 1d). Although the activity is rather low, it is noted that VDF selectivity over  $BaClF$  is high and stable. All these differences are not attributed to the change in specific surface area. Determined by  $N_2$  adsorption and desorption, the specific surface areas of all catalyst samples are rather low ( $< 2\text{ m}^2/\text{g}$ ). We suggest that the specific surface play a minor role in the performance difference of catalysts.

As argued previously, for both  $BaF_2$  or  $BaCl_xF_y$ , the reason for deactivation during the dehydrochlorination reaction is that the catalyst reacts with the HCl generated in the reaction, and then F elements on the catalyst are further replaced by Cl [11]. This is the major contributor to deactivation, in addition to the coke deposition. Clearly, both  $BaCl_xF_y$  and  $BaF_2$  tend to be further chlorinated during the reaction. However,  $BaCl_xF_y$  catalysts exhibit an improved performance, while  $BaF_2$  deactivated relatively rapidly. This may indicate that the  $BaCl_xF_y$  formed during preparation by solid-state reaction at room temperature is not exactly the same as the  $BaCl_xF_y$  formed in the reaction, or after adding Cl in the preparation, it can significantly slow down the speed of catalyst chlorination during the reaction. If the catalyst is quickly chlorinated to  $BaCl_2$ , a decrease in activity is inevitable as the  $BaCl_2$  phase is almost inactive. Aluminum chlorofluoride was confirmed to be an excellent

catalyst for C-F bond activation and F/Cl exchange reaction [18,19]. Similarly, barium chlorofluorides are proper catalysts for the dehydrochlorination of HCFC-142b.

The above discussion is confirmed by the results of XRD. As indicated in Figure 2, BaF<sub>2</sub> and BaClF phase structures were prepared by the simple solid-state reaction between Ba(OH)<sub>2</sub> and NH<sub>4</sub>F/NH<sub>4</sub>Cl at room temperature. The XRD patterns of BaF<sub>2</sub> and BaClF agree well with the standard patterns (ICSD-85-1341 for BaF<sub>2</sub> and ICSD-70-1183 for BaClF). No other impurities are detected by XRD. Clearly, solid-state reaction at room temperature is an effective way for the synthesis of BaF<sub>2</sub> and BaClF [20].

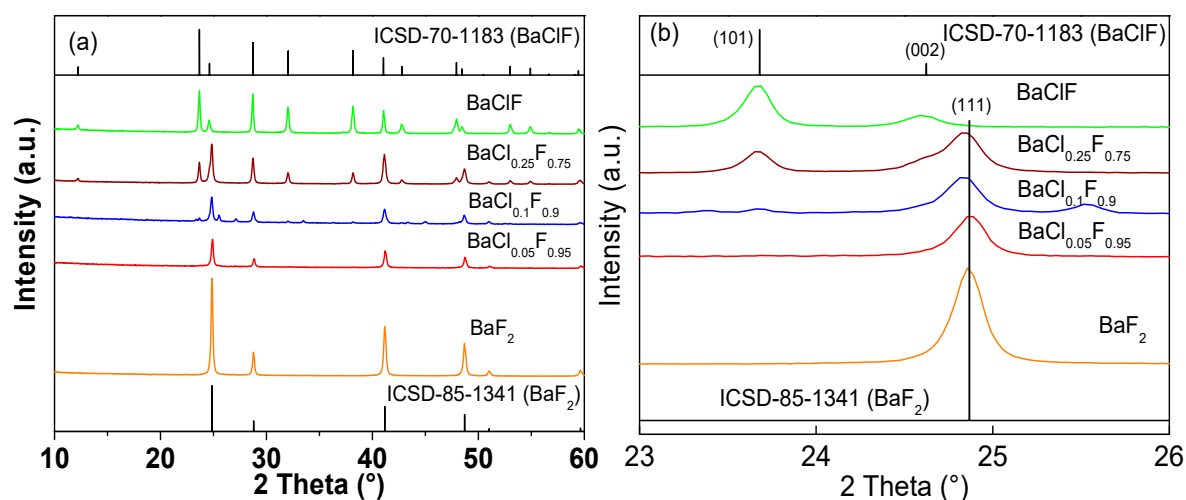


**Figure 2.** (a) XRD patterns of BaF<sub>2</sub> and barium chlorofluoride catalysts before reactions. (b) Highlighted XRD patterns with 2θ between 23° and 26°.

As disclosed in Figure 2a, BaF<sub>2</sub> has a sharp diffraction peak indicating the complete crystallinity. Following the doping of small amounts of Cl, the crystallinity of BaF<sub>2</sub> is weakened significantly. Clearly, during preparation, in addition to the Cl source, the introduction of NH<sub>4</sub>Cl also functions as a template during the formation of BaF<sub>2</sub> particles. Actually, during the process of low-temperature solid-state synthesis, both the particle size and morphology of solid products can be controlled in the presence of proper templates [21–23]. A very weak diffraction of BaClF is observed for BaCl<sub>0.1</sub>F<sub>0.9</sub>. With the further increase in Cl content, the XRD pattern gradually changes from BaF<sub>2</sub> to BaClF, which indicates that the crystal phase of the BaClF is formed continuously after adding Cl, which is more obvious when the Cl content is higher than the BaCl<sub>0.25</sub>F<sub>0.75</sub>, because half of the BaF<sub>2</sub> is transformed into BaClF. In addition to the transformation of the phase structure, the 2θ of BaF<sub>2</sub> shifts following the addition of Cl (Figure 2b). Clearly, the presence of small amounts Cl during solid-state preparation disturbs the formation of BaF<sub>2</sub> crystalline significantly [24,25].

The changes in the crystal structure and surface of the catalysts are further reinforced by TEM images (Figure 3). In the absence of Cl, lattice diffraction fringe (0.362 nm) corresponding to (111) of BaF<sub>2</sub> is detected [26]. In addition to BaF<sub>2</sub>, the BaClF crystal structure with a facet of (101), with a lattice diffraction fringe of 0.376 nm, corresponding to BaClF, is also found for BaCl<sub>0.25</sub>F<sub>0.75</sub>. Over BaClF, only the lattice diffraction fringe spacing of 0.376 nm is identified, indicating the exposure of the (101) plane. This is consistent with the structure evolution revealed in XRD patterns.

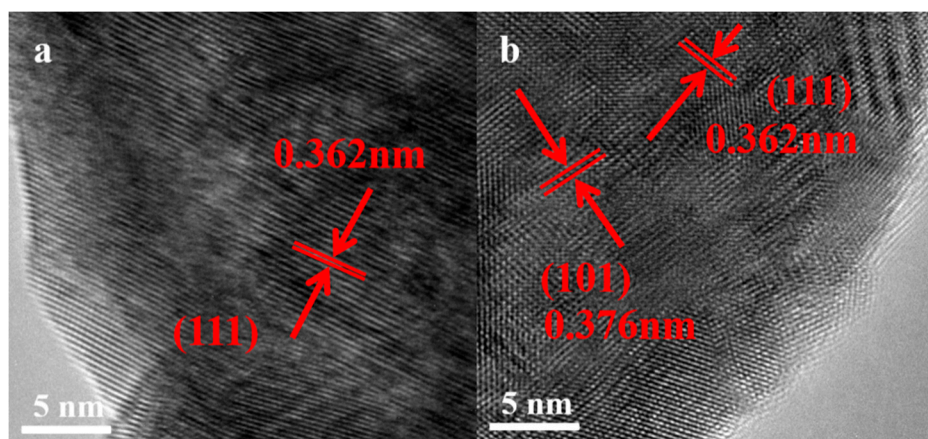


**Figure 3.** High-resolution TEM images of (a)  $\text{BaF}_2$ , (b)  $\text{BaCl}_{0.25}\text{F}_{0.75}$ .

Following reaction (time on stream of 24 h), no formation of  $\text{BaCl}_2$  was detected by XRD (Figure S1). By contrast, the patterns of spent catalysts match with  $\text{BaClF}$  perfectly. This indicates that the  $\text{BaClF}$  structure is relatively stable under reaction conditions (pyrolysis of HCFC-142b 350 °C) after 24 hours of reaction. This shows that the deactivation rate was significantly slowed down and the selectivity to VDF was retained (Figure 1). As  $\text{BaClF}$  phases are obtained for all the spent catalysts, the same activity and selectivity should be achieved. Actually, slight differences in these catalysts are still noticed. Therefore, chlorination of catalysts is not the sole factor for the performance of catalysts.

As shown in Figure 4, the contents of F and Cl of the  $\text{BaCl}_x\text{F}_y$  catalyst before and after reaction were obtained by EDS. The molar ratio of F/Cl after reaction and the calculated ratio of chlorination of the catalyst after reaction are related to the amount of Cl added during the preparation of catalyst. Clearly, the more Cl was added during the preparation, the less F in catalysts was chlorinated. After time on stream of 24 h, over 70% of F was replaced by Cl during the reaction for the  $\text{BaF}_2$  catalyst (Figure 4a). Although no diffraction peak of  $\text{BaCl}_2$  was detected by XRD over the spent catalysts, more Cl than F was quantified by EDS over the spent  $\text{BaF}_2$  catalysts. As illustrated in Figure 4b, the ratio of F/Cl is lower than 0.4, implying the formation of  $\text{BaCl}_2$  species. We suggest that these  $\text{BaCl}_2$  structures are highly dispersed in the catalyst. As a result, these small crystalline particles are not detected by XRD. It is well accepted that the detection limit of XRD is 2–3 nm [27]. Once again, the EDS results confirm that  $\text{BaClF}$  is relatively stable under reaction system. Only small amounts of F were chlorinated during reaction.

With the doping of small amounts of Cl during the catalyst preparation, the chlorination of catalysts during the reaction is significantly inhibited. In addition to  $\text{BaCl}_{0.025}\text{F}_{0.975}$ , the catalysts are maintained at  $\text{BaClF}$  with an F/Cl of close to 1 (Figure 4b). Different from  $\text{BaF}_2$  catalyst, addition of  $\text{NH}_4\text{Cl}$  during catalyst preparation prohibits the catalysts from being further chlorinated to  $\text{BaCl}_2$  following reaction.

As presented in Figure 1,  $\text{BaClF}$  exhibits rather low activity for the conversion of HCFC-142b, although it shows high selectivity to VDF. As  $\text{BaCl}_x\text{F}_y$  catalysts are ultimately chlorinated to  $\text{BaClF}$ , similar activities to  $\text{BaClF}$  should be obtained. However, much higher activities of these catalysts were obtained (Figure 1). Consequently, SEM experiments were carried out for the elucidation of these difference.

As displayed in Figure 5, following solid-state reaction between  $\text{Ba}(\text{OH})_2$  and  $\text{NH}_4\text{F}$  at room temperature, irregular particles were obtained. The particle size ranges from 50 to 300 nm. Although low-temperature solid-state reaction is an effective way to prepare nanomaterials, large  $\text{BaF}_2$  particles were still formed, probably due to the fast fluorination of  $\text{Ba}(\text{OH})_2$  by F ions [28]. However, with the doping of small amounts of  $\text{NH}_4\text{Cl}$ , unexpectedly, much smaller and more uniform particles were achieved for  $\text{BaCl}_{0.025}\text{F}_{0.975}$ . Similarly, in the presence of NaCl, ZnS nanoparticles with a size ranging

from 40 to 80 nm were prepared between the solid-state reaction of  $\text{ZnCl}_2$  and  $\text{Na}_2\text{S}$  [29]. Clearly, both  $\text{NH}_4\text{Cl}$  and  $\text{NaCl}$  can function as templates during the formation of particles via solid state reactions [30]. This result is consistent with the observation of XRD patterns. Following the doping of Cl, the crystal growth of  $\text{BaF}_2$  was inhibited significantly.

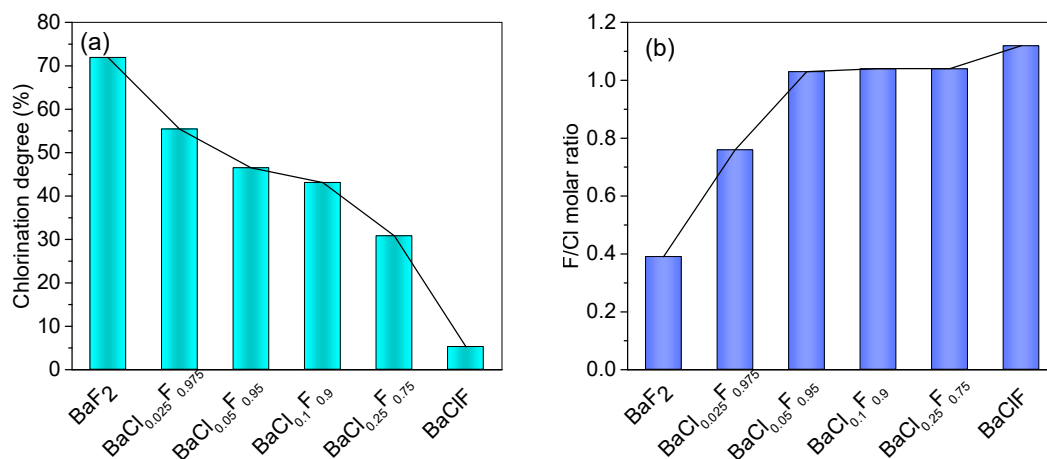


**Figure 4.** Chlorination of catalysts during the pyrolysis of HCFC-142b at 350 °C. (a) Chlorination degree of catalysts after time on stream of 24 h. The chlorination degree is calculated according to the molar ratio of F amount replaced by Cl in the reaction to the amount of F in the fresh catalysts. (b) F/Cl molar ratio in the spent catalysts. The elemental amounts of all the catalysts were determined by EDS technique.

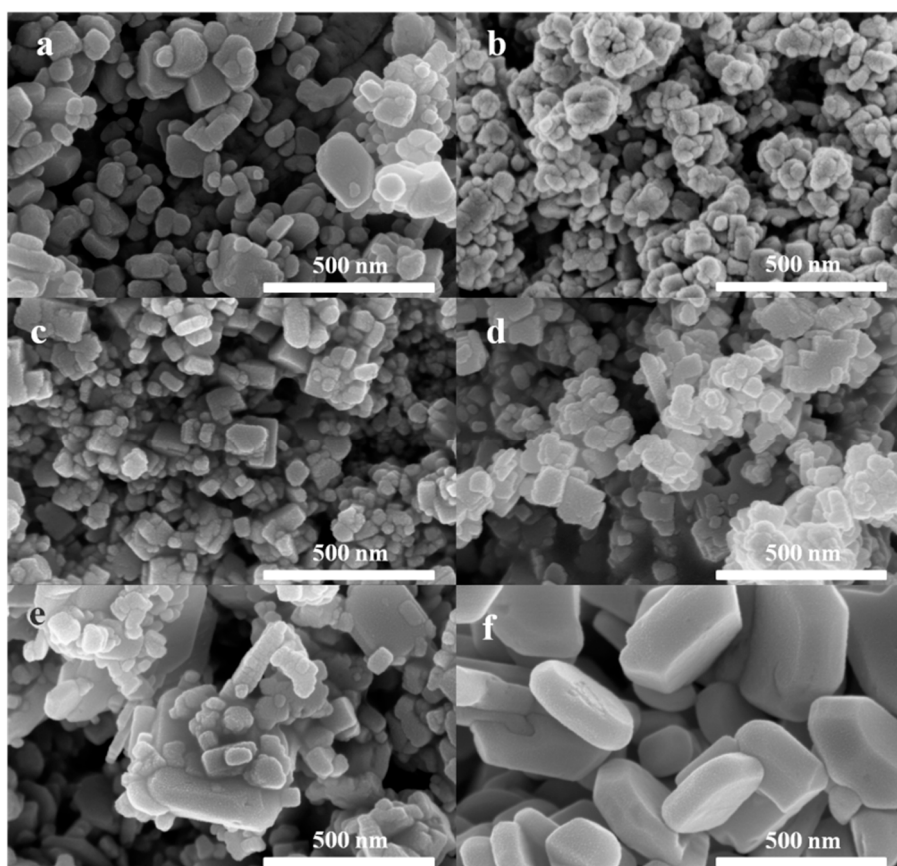


**Figure 5.** SEM images of (a)  $\text{BaF}_2$ , (b)  $\text{BaCl}_{0.025}\text{F}_{0.975}$ , (c)  $\text{BaCl}_{0.05}\text{F}_{0.95}$ , (d)  $\text{BaCl}_{0.1}\text{F}_{0.9}$ , (e)  $\text{BaCl}_{0.25}\text{F}_{0.75}$  and (f)  $\text{BaClF}$ .

With the further doping of  $\text{NH}_4\text{Cl}$  during catalyst preparation, a slight increase in particle size was observed. As presented in Figure 5, the particle size increases with Cl content monotonically. It is worth noting that very large particles for BaClF were obtained, with sizes ranging from 200 to 500 nm. Therefore, the particle size of BaClF is significantly larger than that of  $\text{BaF}_2$  and  $\text{BaCl}_x\text{F}_y$ . We suggest that this mainly contributes to the low activity of the BaClF catalyst.

The morphology of spent catalysts after a time on stream of 24 h is demonstrated in Figure S2. Compared with the SEM images of fresh catalysts (Figure 5), clear sintering is noticed for all the catalysts. Despite the formation of BaClF after reaction, the particle size of the catalyst is still far smaller than that of BaClF and the spent BaClF. Hence, the activity of the  $\text{BaCl}_x\text{F}_y$  catalysts with low Cl content is still much higher than that of the BaClF after reaction.

To verify the effect of crystal size on the catalytic performance, BaClF catalysts were calcined at 300, 400, 500 and 600 °C in air atmosphere. Generally, metal fluorides tend to sinter significantly at elevated temperatures [31,32]. Hence, in the present study, BaClF catalysts were calcined at high temperatures to obtain various crystal sizes. Interestingly, as illustrated in Figure 6, the diffraction of BaClF first decreases with calcination temperature followed by increasing again at temperatures above 400 °C. Consequently, the crystal sizes were determined by the Scherrer equation based on the XRD patterns [33,34]. Prior to the calcination, the crystal size of BaClF was estimated to be around 130.5 nm. Following calcination at 300 °C, the size decreases to 71.5 nm. Following further increases in temperature, the sizes of 52, 74 and 83 nm were obtained for calcination temperatures of 400, 500 and 600 °C respectively. Clearly, relatively low calcination temperatures facilitate the disorder of BaClF structures. As suggested by Kesavamoorthy et al., the interplanar distance of Ba and F planes drops with temperature. By contrast, the Ba and Cl plane is enhanced by elevated temperatures [35,36]. Nevertheless, varied crystal sizes of BaClF were achieved via calcination at different temperatures.

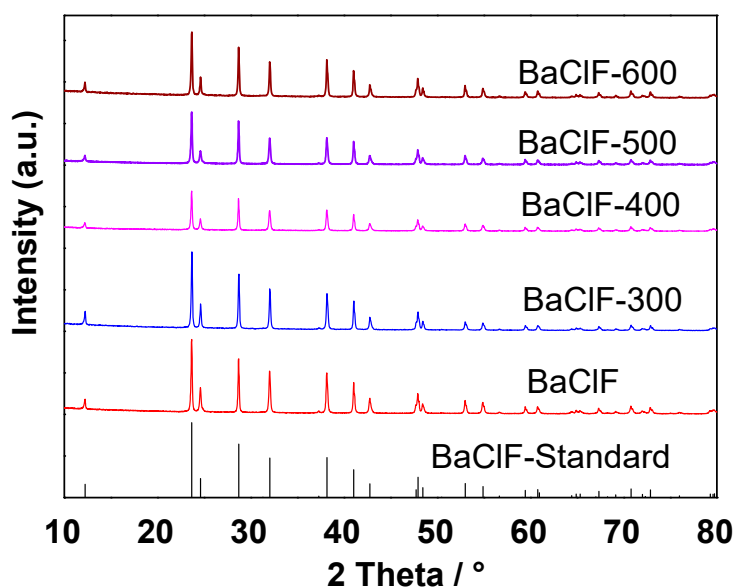


**Figure 6.** XRD patterns BaClF catalysts calcined at temperatures between 300 °C and 600 °C.

Following XRD experiments, the calcined BaClF catalysts were further evaluated for the catalytic pyrolysis of HCFC-142b. The results are displayed in Figure 7. After calcination, the conversion levels of HCFC-142b over BaClF are significantly improved (Figure 7a). Generally, the conversion agrees with the crystal sizes obtained by XRD patterns. BaClF calcined at 400 °C exhibits a relatively high conversion with a small crystal size. Further increases in calcination temperature lead to the sintering of BaClF. Correspondingly, the conversion drops with temperature. As small crystalline particles were obtained following calcination, stable selectivity to VDF is also achieved (Figure 7b).

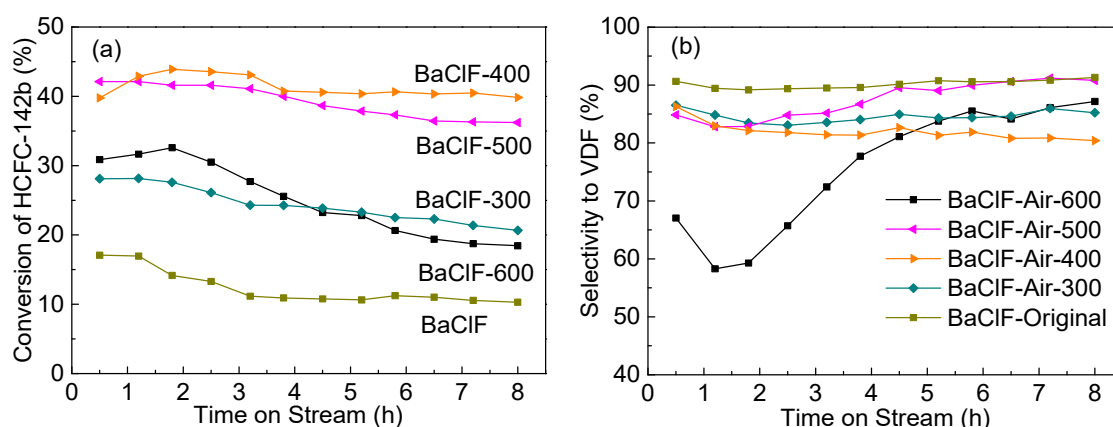


**Figure 7.** Effect of calcination on the conversion of (a) HCFC-142b and (b) selectivity to VDF for BaClF catalysts.

In comparison,  $\text{BaF}_2$  catalysts were also calcined under the same temperatures. As disclosed in Figure S3a, different from BaClF, a strengthening in the diffraction of  $\text{BaF}_2$  is observed at calcination between 300 and 600 °C. According to the calculation, the crystal size of  $\text{BaF}_2$  increases from 42 to 51 and 55 nm after calcination at 400 and 600 °C respectively. Although these catalysts were finally chlorinated to BaClF after reaction (Figure S3b), they still show different catalytic performances. As shown in Figure S4a, the calcination of  $\text{BaF}_2$  leads to a significant decrease in the conversion of HCFC-142b. When calcined at 700 °C,  $\text{BaF}_2$  is almost totally deactivated. However, no clear difference was found for VDF selectivity (Figure S4b).

Based on the above discussion, XRD revealed that a smaller crystal size was achieved following Cl doping (Figure 2). In addition, as confirmed by SEM images (Figure 5), Cl doping also lead to the decrease in the particle size. Hence, we suggest that the particle size or crystal size of a barium catalyst plays a major role in the catalytic performance. Similar results were also confirmed for  $\text{Cr}_2\text{O}_3$  catalysts for the dehydrofluorination of 1,1-difluoroethane [37].

The catalysts were further investigated by XPS characterization and the results are shown in Figure 8. The binding energy of Ba in  $\text{BaF}_2$  was determined to be 795.2 eV, which is consistent with the standard [38,39]. Upon the addition of Cl element to  $\text{BaF}_2$ , a clear shift in Ba  $3d_{3/2}$  towards a higher binding energy is noticed (Figure 8a). Clearly, small amounts of Cl in  $\text{BaF}_2$  not only inhibit the growth of  $\text{BaF}_2$  and BaClF crystalline, but also affect the chemical state of the Ba element. Due to the different interactions of Ba with Cl and F, the fast growth of crystalline is inhibited. In addition to the crystal growth, these differences may also contribute to the improved conversion and selectivity. Due to the change in Ba-binding energy, the adsorption and activation of the C-Cl bond for HCFC-142b are altered. A similar trend is also found for the F 1s spectrum (Figure 8b). Consistent with XRD and TEM results, the XPS spectra of spent catalysts confirm the formation of BaClF during the catalytic pyrolysis of HCFC-142b (Figure S5). In addition to the composition of catalysts, reaction temperature [40], reaction pressure and environment [41] play an important role in the catalytic performance of the pyrolysis process. These issues will be addressed in the future studies after the optimization of the catalysts.

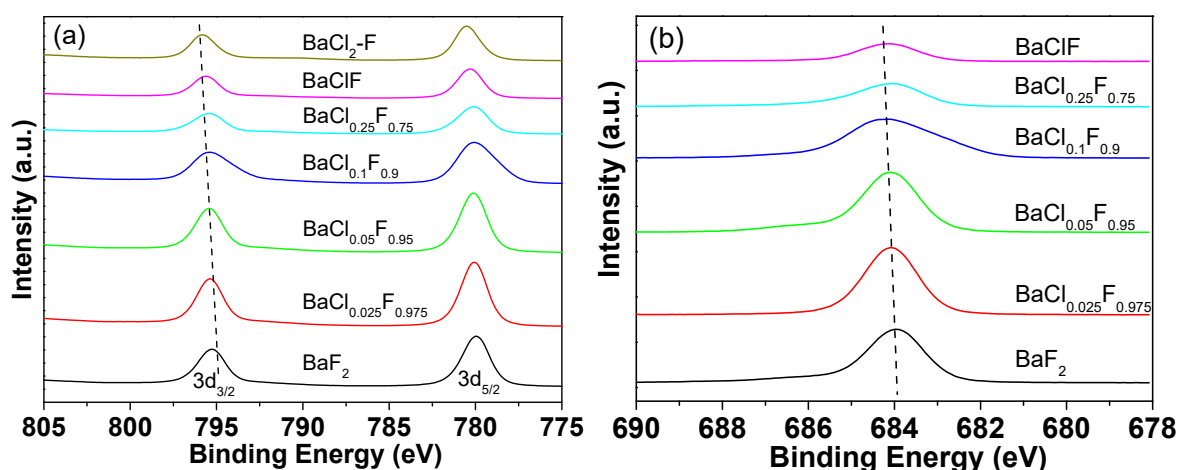


**Figure 8.** High resolution XPS of (a) Ba 3d and (b) F 1s spectra of BaF<sub>2</sub> and barium chlorofluoride catalysts before reactions.

### 3. Materials and Methods

#### 3.1. Preparation of Catalysts

Barium chlorofluoride was synthesized by solid-state grinding method with the reaction between Ba(OH)<sub>2</sub>·8H<sub>2</sub>O, NH<sub>4</sub>F and NH<sub>4</sub>Cl [42,43]. Ba(OH)<sub>2</sub>·8H<sub>2</sub>O, NH<sub>4</sub>F and NH<sub>4</sub>Cl were purchased from Aladdin Co. (Shanghai, China) with analytical purity (>98.0%) without further purification. During the preparation of barium chlorofluoride, a total of 0.1 mol NH<sub>4</sub>F and NH<sub>4</sub>Cl with different proportions were mixed and grinded in a mortar rigorously for 0.5 h. Then, 0.1 mol Ba(OH)<sub>2</sub>·8H<sub>2</sub>O powder was added to the mixture, followed by grinding for a further 1 h. During the grinding, pungent gas was smelt (emission of NH<sub>3</sub>). Following the release of crystal water, wet paste was formed gradually. The paste was dried at 120 °C for 5 h, leading to the formation of barium chlorofluoride. For comparison, neat BaF<sub>2</sub> and BaCl<sub>2</sub> were also prepared following similar procedures. The chemical equation used during preparation is as follows. The conditions of catalyst preparation are listed in Table 1.



**Table 1.** Preparation conditions of catalysts for BaF<sub>2</sub>, barium chlorofluoride and BaCl<sub>2</sub>.

Catalyst	Amounts, mol		
	Ba(OH) <sub>2</sub> ·8H <sub>2</sub> O	NH <sub>4</sub> F	NH <sub>4</sub> Cl
BaF <sub>2</sub>	0.1	0.2	0
BaCl <sub>0.05</sub> F <sub>1.95</sub>	0.1	0.195	0.005
BaCl <sub>0.1</sub> F <sub>1.9</sub>	0.1	0.19	0.01
BaCl <sub>0.2</sub> F <sub>1.8</sub>	0.1	0.18	0.02
BaCl <sub>0.5</sub> F <sub>1.5</sub>	0.1	0.15	0.05
BaClF	0.1	0.1	0.1
BaCl <sub>2</sub>	0.1	0	0.2

#### 3.2. Catalytic Activity

The catalytic activity of BaCl<sub>x</sub>F<sub>y</sub> was evaluated in a tubular fixed-bed reactor. A nickel tube with an inner diameter of 22 mm was adopted as the reactor. Blank experiments confirmed that no reaction was detected in the absence of catalysts. The HCFC-142b (>99.0%, Juhua Co., Zhejiang, China) reaction gas was diluted by equivalent amounts of N<sub>2</sub> (>99.9%, Mingxin Gas Co., Hangzhou, China) which were controlled by mass flow rate controllers (D09-11C, Qixing, Beijing, China) respectively. Prior to

reaction, a 2 mL catalyst with a particle size ranging from 0.425 to 0.850 mm (20–40 mesh) was loaded to the isothermal zone of the reactor. A thermal couple was located in the middle the catalyst bed for the detection of reaction temperature. The reactions were carried out at atmospheric pressure, a gas hourly space velocity (GHSV) of  $1200 \text{ h}^{-1}$  (HCFC-142b and  $\text{N}_2$ ), and a reaction temperature of  $350 \text{ }^\circ\text{C}$ . KOH solution with a concentration of 1 mol/L was used to remove the effluent acid gas (HCl and HF) formed during the reaction. A gas chromatograph (GC-1690 JieDao) equipped with a thermal conductivity detector (TCD) was used to analyze the gas composition.

### 3.3. Catalyst Characterization

X-ray diffraction (XRD) experiments were carried out for the identification of crystal structures. XRD patterns were obtained over an X'Pert Pro analytical instrument (Almelo, Overijssel, The Netherlands). X-Ray photoelectron spectroscopy (XPS) measurements were performed by Thermo EscaLab 250Xi (Cambridge, Massachusetts, USA), equipped with monochromatized Al  $K\alpha$  X-ray as the excitation source (24.2 W). The binding energy values were corrected for charging effect by referring to the adventitious C1s line at 284.5 eV. Scanning electron microscopy (SEM) studies were carried out on a Helios G4 CX (Cambridge, Massachusetts, USA) equipped with an X-ray energy spectrometer (EDS). Transmission Electron Microscope (TEM) studies were carried out on a Tecnai G2 F30 (Hillsboro, Oregon, USA).

## 4. Conclusions

$\text{BaF}_2$  and  $\text{BaCl}_x\text{F}_y$  catalysts were successfully prepared via the solid-state reaction method at room temperature. Both catalysts promote the pyrolysis of HCFC-142b ( $\text{CH}_3\text{CClF}_2$ ) to VDF ( $\text{CH}_2=\text{CF}_2$ ) at  $350 \text{ }^\circ\text{C}$ , which is significantly lower than the industrial manufacture temperature ( $600\text{--}700 \text{ }^\circ\text{C}$ ) by the thermal decomposition of HCFC-142b. However, for the  $\text{BaF}_2$  catalyst, the selectivity of VDF decreases from 94% to 84% along with the deactivation of the  $\text{BaF}_2$  catalyst monotonically. In the presence of small amounts of Cl in  $\text{BaF}_2$ , stabilized selectivity is achieved. Over  $\text{BaCl}_{0.05}\text{F}_{0.95}$ ,  $\text{BaCl}_{0.1}\text{F}_{0.9}$  and  $\text{BaCl}_{0.25}\text{F}_{0.75}$ , no decrease in VDF selectivity is observed. According to XRD results, the presence of small amounts Cl during solid-state preparation disturb the formation of  $\text{BaF}_2$  crystalline significantly. Despite the formation of BaClF after reaction, the particle size of the  $\text{BaCl}_x\text{F}_y$  catalysts are still far smaller than that of BaClF and the spent BaClF. Hence, the activity of the  $\text{BaCl}_x\text{F}_y$  catalysts with a low Cl content is still much higher than that of the BaClF after reaction. We suggest that the particle size, or more precisely, the crystal size of the barium catalyst play a major role in the catalytic performance. In addition to the crystal growth, the presence of small amounts of Cl during catalyst preparation changes the chemical state of Ba, and therefore the adsorption and activation of the C-Cl bond for HCFC-142b are altered.

**Supplementary Materials:** The following are available online at <http://www.mdpi.com/2073-4344/10/4/377/s1>, Figure S1: XRD patterns of spent  $\text{BaF}_2$  and barium chlorofluoride catalysts; Figure S2: XRD patterns  $\text{BaF}_2$  catalysts calcined at temperatures between  $300 \text{ }^\circ\text{C}$  and  $600 \text{ }^\circ\text{C}$ ; Figure S3: XRD patterns  $\text{BaF}_2$  catalysts calcined at temperatures between  $300 \text{ }^\circ\text{C}$  and  $600 \text{ }^\circ\text{C}$ ; Figure S4: Effect of calcination on the conversion of HCFC-142b and selectivity to VDF for  $\text{BaF}_2$  catalysts; Figure S5: High resolution XPS spectra of SEM images of  $\text{BaF}_2$  and barium chlorofluoride catalysts following reaction with time on stream of 24 h.

**Author Contributions:** Conceptualization, W.H.; methodology, W.H. and W.Y.; validation, W.Y., Y.L. (Yongnan Liu), J.L. and H.Y.; formal analysis, W.Y. and B.L.; investigation, W.Y., Y.L. (Yongnan Liu), J.L. and H.Y.; resources, W.H., H.T., A.C. and Y.L. (Ying Li); data curation, W.Y.; writing—original draft preparation, W.Y.; writing—review and editing, W.H.; visualization, W.Y.; supervision, W.H., H.T., A.C. and Y.L. (Ying Li); project administration, W.H.; funding acquisition, W.H. and A.C. All authors have read and agreed to the published version of the manuscript.

**Funding:** This research was supported by Zhejiang Provincial Natural Science Foundation of China under grant no. LY19B060009 and LY19B050004.

**Conflicts of Interest:** The authors declare no conflict of interest. The funders had no role in the design of the study; in the collection, analyses, or interpretation of data; in the writing of the manuscript, or in the decision to publish the results.

## References

1. Ameduri, B. From Vinylidene Fluoride (VDF) to the Applications of VDF-Containing Polymers and Copolymers: Recent Developments and Future Trends. *Chem. Rev.* **2009**, *109*, 6632–6686. [[CrossRef](#)] [[PubMed](#)]
2. Améduri, B.; Boutevin, B.; Kostov, G. Fluoroelastomers: Synthesis, properties and applications. *Prog. Polym. Sci.* **2001**, *26*, 105–187. [[CrossRef](#)]
3. Wang, Z.; Han, W.; Tang, H.; Liu, H. CaBaF<sub>x</sub> composite as robust catalyst for the pyrolysis of 1-chloro-1,1-difluoroethane to vinylidene fluoride. *Catal. Commun.* **2019**, *120*, 42–45. [[CrossRef](#)]
4. Wang, Z.; Han, W.; Liu, H. EDTA-assisted hydrothermal synthesis of cubic SrF<sub>2</sub> particles and their catalytic performance for the pyrolysis of 1-chloro-1,1-difluoroethane to vinylidene fluoride. *Crystengcomm* **2019**, *21*, 1691–1700. [[CrossRef](#)]
5. Zhang, P.Z.; Jiang, Z.B.; Cui, Y.H.; Xie, G.Q.; Jin, Y.Z.; Guo, L.L.; Xu, Y.Q.; Zhang, Q.F.; Li, X.N. Catalytic performance of ionic liquid for dehydrochlorination reaction: Excellent activity and unparalleled stability. *Appl. Catal. B Environ.* **2019**, *255*, 10. [[CrossRef](#)]
6. Sun, X.; Liu, X.; Qin, Y.C.; Qiang, L.; He, Y.P.; Su, D.S.; Song, L.J.; Sun, Z.L. Direct Conversion of Acetylene and 1,2-Dichloroethane to Vinyl Chloride Monomer over a Supported Carbon Nitride Catalyst: Tunable Activity Controlled by the Synthesis Temperature. *Ind. Eng. Chem. Res.* **2019**, *58*, 5404–5413. [[CrossRef](#)]
7. Mao, W.; Bai, Y.; Wang, W.; Wang, B.; Xu, Q.; Shi, L.; Li, C.; Lu, J. Highly Selective Dehydrochlorination of 1,1,1,2-Tetrafluoro-2-chloropropane to 2,3,3,3-Tetrafluoropropene over Alkali Metal Fluoride Modified MgO Catalysts. *ChemCatChem* **2017**, *9*, 824–832. [[CrossRef](#)]
8. Scharfe, M.; Zichittella, G.; Kondratenko, V.A.; Kondratenko, E.V.; Lopez, N.; Perez-Ramirez, J. Mechanistic origin of the diverging selectivity patterns in catalyzed ethane and ethene oxychlorination. *J. Catal.* **2019**, *377*, 233–244. [[CrossRef](#)]
9. Wang, Z.; Han, W.; Zhang, C.; Zhou, S.; Wang, H.; Tang, H.; Liu, H. Preparation of N-Doped Activated Carbon for Catalytic Pyrolysis of 1-Chloro-1,1-difluoroethane to Vinylidene Fluoride. *Chemistryselect* **2018**, *3*, 1015–1018. [[CrossRef](#)]
10. Wang, Z.; Han, W.; Tang, H.; Li, Y.; Liu, H. Preparation of N-doped ordered mesoporous carbon and catalytic performance for the pyrolysis of 1-chloro-1,1-difluoroethane to vinylidene fluoride. *Microporous Mesoporous Mater.* **2019**, *275*, 200–206. [[CrossRef](#)]
11. Han, W.; Liu, B.; Kang, Y.; Wang, Z.; Yu, W.; Yang, H.; Liu, Y.; Lu, J.; Tang, H.; Li, Y.; et al. Experimental and DFT Mechanistic Study of Dehydrohalogenation of 1-Chloro-1,1-difluoroethane over Metal Fluorides. *Ind. Eng. Chem. Res.* **2019**, *58*, 18149–18159. [[CrossRef](#)]
12. Han, W.; Zhang, C.; Wang, H.; Zhou, S.; Tang, H.; Yang, L.; Wang, Z. Sub-nano MgF<sub>2</sub> embedded in carbon nanofibers and electrospun MgF<sub>2</sub> nanofibers by one-step electrospinning as highly efficient catalysts for 1,1,1-trifluoroethane dehydrofluorination. *Catal. Sci. Technol.* **2017**, *7*, 6000–6012. [[CrossRef](#)]
13. Han, W.; Wang, H.; Liu, B.; Li, X.; Tang, H.; Li, Y.; Liu, H. PVDF mediated fabrication of freestanding AlF<sub>3</sub> sub-microspheres: Facile and controllable synthesis of alpha, beta and theta-AlF<sub>3</sub>. *Mater. Chem. Phys.* **2020**, *240*. [[CrossRef](#)]
14. Liu, B.; Han, W.; Li, X.; Li, L.; Tang, H.; Lu, C.; Li, Y.; Li, X. Quasi metal organic framework with highly concentrated Cr<sub>2</sub>O<sub>3</sub> molecular clusters as the efficient catalyst for dehydrofluorination of 1,1,1,3,3-pentafluoropropane. *Appl. Catal. B Environ.* **2019**, *257*. [[CrossRef](#)]
15. Calvo, B.; Marshall, C.P.; Krahl, T.; Krohnert, J.; Trunschke, A.; Scholz, G.; Braun, T.; Kemnitz, E. Comparative study of the strongest solid Lewis acids known: ACF and HS-AlF<sub>3</sub>. *Dalton Trans.* **2018**, *47*, 16461–16473. [[CrossRef](#)]
16. Fang, X.-X.; Wang, Y.; Jia, W.-Z.; Song, J.-D.; Wang, Y.-J.; Luo, M.-F.; Lu, J.-Q. Dehydrofluorination of 1, 1, 1, 3, 3-pentafluoropropane over C-AlF<sub>3</sub> composite catalysts: Improved catalyst stability by the presence of pre-deposited carbon. *Appl. Catal. Gen.* **2019**, *576*, 39–46. [[CrossRef](#)]
17. Teinz, K.; Wuttke, S.; Boerno, F.; Eicher, J.; Kemnitz, E. Highly selective metal fluoride catalysts for the dehydrohalogenation of 3-chloro-1,1,1,3-tetrafluorobutane. *J. Catal.* **2011**, *282*, 175–182. [[CrossRef](#)]
18. Meissner, G.; Dirican, D.; Jager, C.; Braun, T.; Kemnitz, E. Et<sub>3</sub>GeH versus Et<sub>3</sub>SiH: Controlling reaction pathways in catalytic C-F bond activations at a nanoscopic aluminum chlorofluoride. *Catal. Sci. Technol.* **2017**, *7*, 3348–3354. [[CrossRef](#)]

19. Krahl, T.; Kemnitz, E. The very strong solid Lewis acids aluminium chlorofluoride (ACF) and bromofluoride (ABF)—Synthesis, structure, and Lewis acidity. *J. Fluor. Chem.* **2006**, *127*, 663–678. [[CrossRef](#)]
20. Yu, Y.; Jia, D.Z.; Ge, W.W.; Jin, C.F.; Xin, X.Q. Synthesis of inorganic nano-materials by solid state reaction at low-heating temperatures. *Chin. J. Inorg. Chem.* **2004**, *20*, 881–888.
21. Liu, X.H.; Yu, L. Synthesis of nanosized nickel hydroxide by solid-state reaction at room temperature. *Mater. Lett.* **2004**, *58*, 1327–1330. [[CrossRef](#)]
22. Yu, X.H.; Li, F.; Ye, X.R.; Xin, X.Q.; Xue, Z.L. Synthesis of cerium(IV) oxide ultrafine particles by solid-state reactions. *J. Am. Ceram. Soc.* **2000**, *83*, 964–966. [[CrossRef](#)]
23. Sun, Z.P.; Liu, L.; Zhang, L.; Jia, D.Z. Rapid synthesis of ZnO nano-rods by one-step, room-temperature, solid-state reaction and their gas-sensing properties. *Nanotechnology* **2006**, *17*, 2266–2270. [[CrossRef](#)]
24. Wang, X.L.; Liu, Z.Q.; Stevens-Kalceff, M.A.; Riesen, H. Mechanochemical Preparation of Nanocrystalline BaFCl Doped with Samarium in the 2+ Oxidation State. *Inorg. Chem.* **2014**, *53*, 8839–8841. [[CrossRef](#)]
25. Hagemann, H.; D’Anna, V.; Daku, M.L.; Kubel, F. Crystal Chemistry in the Barium Fluoride Chloride System. *Cryst. Growth Des.* **2012**, *12*, 1124–1131. [[CrossRef](#)]
26. Chialanza, M.R.; Schneider, J.F.; Keuchkerian, R.; Romero, M.; Faccio, R.; Olivera, A.; Pereira, H.B. Structural analysis of oxyfluoride borate glass and BaF<sub>2</sub> crystallization from phase separation. *J. Am. Ceram. Soc.* **2020**, *103*, 3126–3137. [[CrossRef](#)]
27. Saowadee, N.; Agersted, K.; Bowen, J.R. Lattice constant measurement from electron backscatter diffraction patterns. *J. Microsc.* **2017**, *266*, 200–210. [[CrossRef](#)]
28. Radmilovic, V.; Ophus, C.; Marquis, E.A.; Rossell, M.D.; Tolley, A.; Gautam, A.; Asta, M.; Dahmen, U. Highly monodisperse core-shell particles created by solid-state reactions. *Nat. Mater.* **2011**, *10*, 710–715. [[CrossRef](#)]
29. Lan, C.; Hong, K.Q.; Wang, W.Z.; Wang, G.H. Synthesis of ZnS nanorods by annealing precursor ZnS nanoparticles in NaCl flux. *Solid State Commun.* **2003**, *125*, 455–458. [[CrossRef](#)]
30. Li, F.; Yu, X.H.; Pan, H.J.; Wang, M.L.; Xin, X.Q. Syntheses of MO<sub>2</sub> (M = Si, Ce, Sn) nanoparticles by solid-state reactions at ambient temperature. *Solid State Sci.* **2000**, *2*, 767–772. [[CrossRef](#)]
31. Mao, W.; Bai, Y.; Wang, B.; Wang, W.; Ma, H.; Qin, Y.; Li, C.; Lu, J.; Liu, Z.W. A facile sol-gel synthesis of highly active nano alpha-aluminum fluoride catalyst for dehydrofluorination of hydrofluorocarbons. *Appl. Catal. B Environ.* **2017**, *206*, 65–73. [[CrossRef](#)]
32. Jia, Z.H.; Mao, W.; Bai, Y.B.; Wang, B.; Ma, H.; Li, C.; Lu, J. Hollow nano-MgF<sub>2</sub> supported catalysts: Highly active and stable in gas-phase dehydrofluorination of 1,1,1,3,3-pentafluoropropane. *Appl. Catal. B Environ.* **2018**, *238*, 599–608. [[CrossRef](#)]
33. Mozafari, M.; Moztarzadeh, F.; Tahriri, M. Green synthesis and characterisation of spherical PbS luminescent micro- and nanoparticles via wet chemical technique. *Adv. Appl. Ceram.* **2011**, *110*, 30–34. [[CrossRef](#)]
34. Drits, V.; Srodon, J.; Eberl, D.D. XRD measurement of mean crystalline thickness of illite and illite/smectite: Reappraisal of the Kubler index and the Scherrer equation. *Clay Min.* **1997**, *45*, 461–475. [[CrossRef](#)]
35. Kesavamoorthy, R.; Sundarakkannan, B.; Rao, G.V.N.; Sastry, V.S. Thermal effect on BaFCl: High-temperature X-ray diffraction. *Thermochim. Acta* **1997**, *307*, 185–195. [[CrossRef](#)]
36. Sundarakkannan, B.; Kesavamoorthy, R.; Nisha, J.A.; Sridharan, V.; Sivakumar, T. Antiferroelectric-to-paraelectric transition in BaFCl. *Phys. Rev. B* **1998**, *57*, 11632–11638. [[CrossRef](#)]
37. Han, W.F.; Wang, Z.K.; Li, X.J.; Tang, H.D.; Xi, M.; Li, Y.; Liu, H.Z. Solution combustion synthesis of nano-chromia as catalyst for the dehydrofluorination of 1,1-difluoroethane. *J. Mater. Sci.* **2016**, *51*, 11002–11013. [[CrossRef](#)]
38. Andrade, A.B.; Ferreira, N.S.; Valerio, M.E.G. Particle size effects on structural and optical properties of BaF<sub>2</sub> nanoparticles. *RSC Adv.* **2017**, *7*, 26839–26848. [[CrossRef](#)]
39. Au, C.T.; Chen, K.D.; Ng, C.F. Characterization of BaX<sub>2</sub>/Gd<sub>2</sub>O<sub>3</sub> (X = F, Cl, Br) catalysts for the oxidative coupling of methane. *Appl. Catal. Gen.* **1998**, *171*, 283–291. [[CrossRef](#)]
40. Laws, P.A.; Hayley, B.D.; Anthony, L.M.; Roscoe, J.M. Kinetic study of the mechanism of the low-temperature pyrolysis of vinyl bromide. *J. Phys. Chem.* **2001**, *105*, 1830–1837. [[CrossRef](#)]
41. Kunsagi-Mate, S.; Vegh, E.; Nagy, G.; Kollar, L. Influence of the molecular environment on the three-center versus four-center elimination of HBr from vinyl bromide: A theoretical approach. *J. Phys. Chem.* **2002**, *106*, 6319–6324. [[CrossRef](#)]

42. Hu, P.; Cao, Y.; Jia, D.; Li, Q.; Liu, R. Engineering the metathesis and oxidation-reduction reaction in solid state at room temperature for nanosynthesis. *Sci. Rep.* **2014**, *4*. [[CrossRef](#)] [[PubMed](#)]
43. Al-Terkawi, A.A.; Scholz, G.; Emmerling, F.; Kemnitz, E. Mechanochemical Synthesis, Characterization, and Structure Determination of New Alkaline Earth Metal-Tetrafluoroterephthalate Frameworks. *Cryst. Growth Des.* **2016**, *16*, 1923–1933. [[CrossRef](#)]



© 2020 by the authors. Licensee MDPI, Basel, Switzerland. This article is an open access article distributed under the terms and conditions of the Creative Commons Attribution (CC BY) license (<http://creativecommons.org/licenses/by/4.0/>).